PCCP

PAPER

Two novel silicon phases with direct band gaps

Qingyang Fan,[a] Changchun Chai,[a] Qun Wei*[b] and Yintang Yang[a]

Cite this: *Phys. Chem. Chem. Phys.*, 2016, **18**, 12905

Received 11th January 2016,
Accepted 23rd March 2016

DOI: 10.1039/c6cp00195e

www.rsc.org/pccp

Due to its abundance, silicon is the preferred solar-cell material despite the fact that many silicon allotropes have indirect band gaps. Elemental silicon has a large impact on the economy of the modern world and is of fundamental importance in the technological field, particularly in the solar cell industry. Looking for direct band gap silicon is still an important field in material science. Based on density function theory with the ultrasoft pseudopotential scheme in the frame of the local density approximation and the generalized gradient approximation, we have systematically studied the structural stability, absorption spectra, electronic, optical and mechanical properties and minimum thermal conductivity of two novel silicon phases, *Cm*-32 silicon and $P2_1/m$ silicon. These are both thermally, dynamically and mechanically stable. The absorption spectra of *Cm*-32 silicon and $P2_1/m$ silicon exhibit significant overlap with the solar spectrum and thus, excellent photovoltaic efficiency with great improvements over $Fd\bar{3}m$ Si. These two novel Si structures with direct band gaps could be applied in single p–n junction thin-film solar cells or tandem photovoltaic devices.

I. Introduction

Due to the limited supply of fossil fuels and their adverse effect on the environment, to find clean and sustainable energy sources is one of the most arduous and significant challenges of the 21st century. Of all the renewable energy sources available, solar energy is the best solution,[1] but development of efficient photovoltaic materials to convert solar energy into electricity is essential. Silicon, because of its high abundance and stability, has been widely used as a photovoltaic material for solar cell devices. However, $Fd\bar{3}m$ silicon does not absorb sunlight as efficiently as some other materials do. Its indirect band gap of 1.12 eV significantly limits the efficiency of solar cells, and its direct band gap of 3.4 eV is too large[2] and only allows high energy photons to be absorbed. Metastable silicon allotropes, such as *R*8, *T*12, *C*2/*m*-16, *C*2/*m*-20, *Amm*2, $I\bar{4}$, $P222_1$ and lonsdaleite structures also exhibit indirect band gaps,[3–8] and BC8 phases show semimetal features.[3,9] None of these materials are suitable for solar absorption. These limitations have led to a constant search for novel silicon structures with appropriate direct band gaps and desired optical properties.

Recently, Botti *et al.*[10] presented first-principles calculations of the electronic and optical properties of silicon allotropes with quasidirect and dipole-allowed band gaps in the range of 0.8–1.5 eV for applications in thin-film solar cells. They all consist of distorted sp^3 silicon networks and have a lower formation energy. By combining the new method with first principles calculations, Xiang *et al.*[11] predicted a new metastable Si_{20}-T structure (space group: $P2_13$) with good optical properties and a quasidirect gap of 1.55 eV. By combining the conformational space annealing (CSA) method[12,13] for global optimization and first-principles density functional calculations, Lee *et al.*[14] predicted some crystalline silicon phases with direct gaps and quasidirect gap structures. D135 silicon (space group: *Cc*) is a direct band gap semiconductor and Q135 silicon (space group: *C*2/*c*) is an indirect band gap semiconductor, the band gap of D135 silicon and Q135 silicon is 1.05 and 1.31 eV with G_0W_0 calculations,[15,16] respectively. D135 silicon exhibits a significant overlap with the solar spectrum and thus, excellent photovoltaic efficiency with great improvements over amorphous Si, polycrystalline Si, and $Fd\bar{3}m$ Si. The D262 phase was also first predicted in ref. 14, namely $P2_1/m$ silicon in this paper. Wang *et al.*, utilizing *ab initio* calculations at ambient pressure, found six metastable allotropes of silicon with direct or quasidirect band gaps of 0.39–1.25 eV.[17] They not only have a direct band gap or quasidirect band gap, but also have better optical properties than the $Fd\bar{3}m$ silicon. Mujica *et al.*[18] found that the *Pbam* structure in carbon, silicon and germanium has a low-energy, low-density metastable polymorph, and *Pbam* silicon is a direct band gap semiconductor with band gap of 1.4 eV. $P4_12_12$ silicon is a likely candidate for the structure of the unknown phase XIII of silicon, $P4_2/ncm$ silicon and $P4_12_12$ silicon are both indirect band gap semiconductors with band gaps of 1.34 eV and 1.77 eV, respectively. The 44 metastable phases of silicon are calculated by Amsler *et al.*[19] using density

[a] *Key Laboratory of Ministry of Education for Wide Band-Gap Semiconductor Materials and Devices, School of Microelectronics, Xidian University, Xi'an 710071, P. R. China*
[b] *School of Physics and Optoelectronic Engineering, Xidian University, Xi'an 710071, P. R. China. E-mail: weiaqun@163.com*

functional theory, of which 11 exhibit direct or quasidirect band gaps in the range of about 1.0–1.8 eV, close to the optimal Shockley–Queisser limit of about 1.4 eV, with a stronger overlap of the absorption spectra with the solar spectrum compared to conventional $Fd\bar{3}m$ silicon. In the study of Guo *et al.*,[20] they found a missing structure, the h-Si6 (space group: $P6_3/mmc$) phase of silicon, by using silicon triangles as the building block. Using first-principles calculations, they confirmed that it has thermal, dynamical, and mechanical stability. h-Si6 silicon is a direct band gap semiconductor with a band gap of 0.61 eV and remarkable optical properties. Oh *et al.*[21] have discovered low-energy pure-Si superlattice structures with dipole-allowed direct band gaps, as well as indirect band gaps, which can be applied to the solar cell industry and pure Si-based optoelectronic devices.

In the present work, we predict two novel silicon allotropes, *Cm*-32 and $P2_1/m$ silicon, whose structure is based on *Cm*-32 and $P2_1/m$ carbon,[22] with silicon atoms substituting the carbon atoms. $P2_1/m$ silicon, in ref. 14 and 23, is based on the conformational space annealing method, while it is based on the transmutation approach in the present manuscript. *Cm*-32 and $P2_1/m$ carbon both have direct band gaps, and better optical properties than $Fd\bar{3}m$ silicon. In addition, the stability, structure, elasticity, elastic anisotropy and minimum thermal conductivity are also systematically investigated.

II. Computational details

A density functional theory (DFT)[24,25] calculation within Vanderbilt ultrasoft pseudopotentials[26] was performed using the Cambridge Serial Total Energy Package (CASTEP) code.[27] For the exchange and correlation functionals, we use the Perdew–Burke–Ernzerhof (PBE) version of the generalized gradient approximation (GGA)[28] and local density approximation (LDA).[29,30] The equilibrium crystal structures were achieved utilizing geometry optimization in the Broyden–Fletcher–Goldfarb–Shanno (BFGS)[31] minimization scheme. For *Cm*-32 silicon, $P2_1/m$ silicon and $Fd\bar{3}m$ silicon, the energy cutoff of 360 eV was used for the wave function expansions. The high density *k*-point[32] sampling with the grid spacing less than $2\pi \times 0.025$ Å^{-1} ($9 \times 3 \times 5$ for *Cm*-32 silicon, $5 \times 11 \times 7$ for $P2_1/m$ silicon, $8 \times 8 \times 8$ for $Fd\bar{3}m$ silicon) in the Brillouin zone was used. The self-consistent convergence of the total energy is 5×10^{-6} eV per atom; the maximum force on the atom is 0.01 eV Å^{-1}, the maximum ionic displacement was within 5×10^{-4} Å and the maximum stress was within 0.02 GPa. Both HSE06 hybrid functional[33] and GGA-PBE methods were used for the calculation of electronic structures.

III. Results and discussion

Structures

The crystal structures of *Cm*-32 silicon and $P2_1/m$ silicon are shown in Fig. 1. *Cm*-32 silicon has 32 atoms in a conventional cell with the *Cm* (No. 8) structure in monoclinic symmetry and $P2_1/m$ silicon belongs to the $P2_1/m$ (No. 11) space group containing

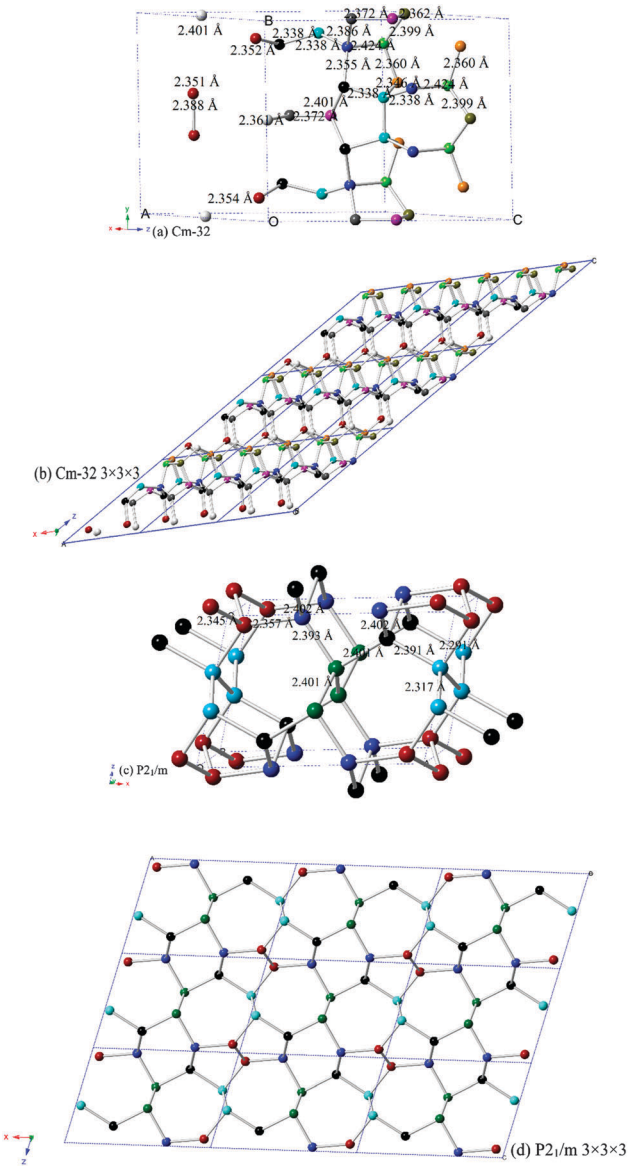

Fig. 1 Unit cell crystal structures of novel silicon allotropes, *Cm*-32 silicon (a and b) and $P2_1/m$ silicon (c and d).

only 10 silicon atoms per conventional cell in monoclinic symmetry. For *Cm*-32 silicon, within this structure, ten inequivalent atoms occupy the crystallographic 4b and 2a sites in the conventional cell, which are 4b (0.3492 0.1037 0.1458), 4b (0.3552 0.3441 0.9311), 4b (0.3488 0.1501 0.9820), 4b (0.8084 0.1539 0.4815), 4b (0.5108 0.1564 0.6035), 4b (0.8358 0.1004 0.6575), 2a (0.6702 0.0 0.0930), 2a (0.1163 0.0 0.5850), 2a (0.6557 0.0 0.9164) and 2a (0.1603 0.0 0.4405). For $P2_1/m$ silicon, five inequivalent atoms occupy the crystallographic 2e site in the conventional cell, which are (0.9397 0.750 0.0877), (0.2975 0.750 0.1926), (0.0361 0.750 0.3963), (0.6907 0.750 0.0428) and (0.5053 0.250 0.61341). At zero pressure, for *Cm*-32 silicon and $P2_1/m$ silicon, their equilibrium lattice constants calculated from GGA (LDA) are a = 8.857 (8.714) Å, b = 11.516 (11.328) Å, c = 14.008 (13.782) Å, β = 151.012° (151.027°) and a = 9.119

(8.960) Å, b = 3.865 (3.797) Å, c = 6.160 (6.066) Å, β = 75.066° (74.853°), respectively. There are 15 bond lengths and 8 bond lengths in the conventional cell of *Cm*-32 silicon and $P2_1/m$ silicon (see Fig. 1(a) and (c)), respectively. The average bond length is 2.371 Å and 2.369 Å for *Cm*-32 silicon and $P2_1/m$ silicon, respectively, they are both slightly larger than that of $Fd\bar{3}m$ silicon (2.352 Å). So we can expect the hardness of $Fd\bar{3}m$ silicon to be larger than that of $P2_1/m$ silicon, and *Cm*-32 silicon to have the smallest hardness of them all. Five-, six- and eight-membered silicon rings are normal to have in the structure of *Cm*-32 silicon and $P2_1/m$ silicon has five-, six- and seven-membered silicon rings (see Fig. 1(b) and (d)). The candidate structures with good porous properties are obtained by stacking different silicon multiple ring units.

Stabilities of novel phases

There are two new phases of Si at ambient pressure which have not been reported yet. To investigate the possible phase transition sequence at ambient pressure, we first calculated the enthalpies of the *Cm*-32 and $P2_1/m$ phases and other silicon phases relative to the $Fd\bar{3}m$ phase. The enthalpies of the *Cm*-32 and $P2_1/m$ phases, together with previously reported new silicon phases, as a function of pressure are shown in Fig. 2. The relative enthalpies are calculated by the formula: $\Delta H = H_{\text{novel phase}}/n_1 - H_{Fd\bar{3}m\text{ phase}}/n_2$, where n_1 is the number of atoms in a conventional cell of the two silicon phases and n_2 is the number of atoms in a conventional cell of $Fd\bar{3}m$ phase. The calculated lattice parameters of *Cm*-32 silicon, $P2_1/m$ silicon and $Fd\bar{3}m$ silicon are listed in Table 1. From Table 1, the $Fd\bar{3}m$ phase is the most stable phase at ambient pressure. Among them, the most unfavorable $P2_1/m$ phase is higher in energy than the $Fd\bar{3}m$ phase by 0.084 eV per atom at ambient pressure, while the more stable *Cm*-32 phase is 0.072 eV per atom higher than the $Fd\bar{3}m$ phase. In ref. 17 and in this work, the most unfavorable tP16-Si is higher in energy than $Fd\bar{3}m$ silicon by 0.269 eV per atom and by 0.277 eV per atom at zero pressure, but tP16-Si is still mechanically and dynamically stable. Then, the dynamical and

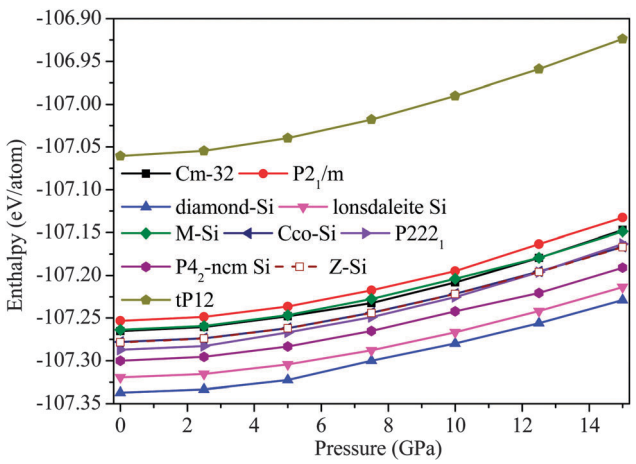

Fig. 2 Calculated enthalpies of different silicon structures as a function of pressure.

Table 1 The calculated lattice parameters and relative enthalpy per atom of *Cm*-32 silicon, $P2_1/m$ silicon and $Fd\bar{3}m$ silicon

Space group		a (Å)	b (Å)	c (Å)	β (°)	Energy/atom (eV per atom)
Cm-32	GGA	8.857	11.516	14.008	151.012	0.072
	LDA	8.714	11.328	13.782	151.027	
$P2_1/m$	GGA	9.119	3.865	6.160	75.066	0.084
	LDA	8.960	3.797	6.066	74.853	
$Fd\bar{3}m$	GGA	5.442				0.000
	LDA	5.418				
	Exp.	5.431[a]				

[a] Ref. 61.

mechanical stability of *Cm*-32 silicon and $P2_1/m$ silicon was checked. The calculated phonon spectra of *Cm*-32 silicon and $P2_1/m$ silicon are shown in Fig. 3. No imaginary frequencies are observed throughout the whole Brillouin zone, signaling dynamical and structural stability of *Cm*-32 silicon and $P2_1/m$ silicon. The mechanical stabilities are checked using the elastic constants of *Cm*-32 silicon and $P2_1/m$ silicon. Utilizing the strain–stress relationship, we calculated the elastic constants of *Cm*-32 silicon and $P2_1/m$ silicon. Due to the monoclinic symmetry of *Cm*-32 silicon and $P2_1/m$ silicon there are thirteen independent elastic constants C_{ij}, namely C_{11}, C_{12}, C_{13}, C_{15}, C_{22}, C_{23}, C_{25}, C_{33}, C_{35}, C_{44}, C_{46}, C_{55}, and C_{66}. For a stable monoclinic structure, its thirteen independent elastic constants should obey the following generalized Born's mechanical stability criteria:[34,35]

$$C_{ii} > 0, \quad i = 1\text{–}6, \tag{1}$$

$$[C_{11} + C_{22} + C_{33} + 2(C_{12} + C_{13} + C_{23})] > 0, \tag{2}$$

$$(C_{33}C_{55} - C_{35}^2) > 0, \tag{3}$$

$$(C_{44}C_{66} - C_{46}^2) > 0, \tag{4}$$

$$(C_{22} + C_{33} - 2C_{23}) > 0, \tag{5}$$

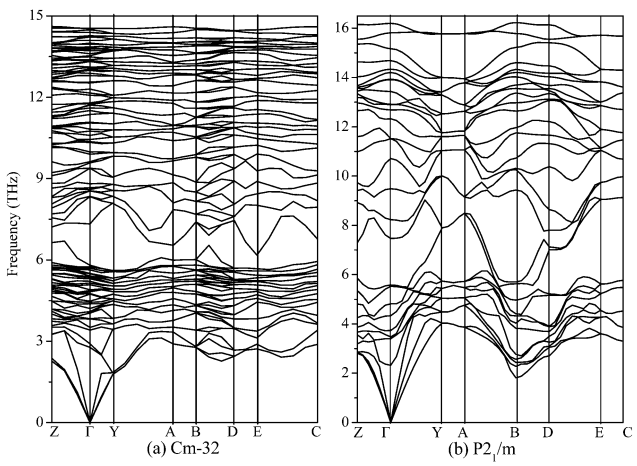

Fig. 3 Phonon spectra for *Cm*-32 silicon (a) and $P2_1/m$ silicon (b).

Table 2 The calculated elastic constants (GPa) of *Cm*-32 silicon, $P2_1/m$ silicon and $Fd\bar{3}m$ silicon

Space group	C_{11}	C_{12}	C_{13}	C_{15}	C_{22}	C_{23}	C_{25}	C_{33}	C_{35}	C_{44}	C_{46}	C_{55}	C_{66}
Cm-32	137	41	52	2	159	40	−9	152	0.5	40	−2	52	40
$P2_1/m$	147	27	50	12	165	47	−5	155	5	69	−2	55	38
$Fd\bar{3}m$	154	56								79			
	166[a]	64								80			

[a] Ref. 62 – experimental, at 300 K.

$$[C_{22}(C_{33}C_{55} - C_{35}^2) + 2C_{23}C_{25}C_{35} - C_{23}^2C_{55} - C_{25}^2C_{33}] > 0, \quad (6)$$

$$\Omega = 2[C_{15}C_{25}(C_{33}C_{12} - C_{13}C_{23}) + C_{15}C_{35}(C_{22}C_{13} - C_{12}C_{33}) + C_{25}C_{35}(C_{11}C_{23} - C_{12}C_{13})] - [C_{15}^2(C_{22}C_{33} - C_{23}^2) + C_{25}^2(C_{11}C_{33} - C_{13}^2) + C_{35}^2(C_{11}C_{22} - C_{12}^2)] + C_{55}g > 0 \quad (7)$$

$$g = C_{11}C_{22}C_{33} - C_{11}C_{23}^2 - C_{22}C_{13}^2 - C_{33}C_{12}^2 + 2C_{12}C_{13}C_{23} \quad (8)$$

The calculated elastic constants of *Cm*-32 silicon, $P2_1/m$ silicon and $Fd\bar{3}m$ silicon are listed in Table 2. The calculated elastic constants of $Fd\bar{3}m$ silicon are in excellent agreement with the available experimental values, which indicates that our calculations are valid and believable. The elastic constants under ambient pressure of *Cm*-32 silicon and $P2_1/m$ silicon satisfy Born's mechanical stability criteria of monoclinic symmetry. That is to say, *Cm*-32 silicon and $P2_1/m$ silicon are mechanically stable.

Mechanical properties

The elastic modulus is defined as the slope of its stress–strain curve in the elastic deformation region:[36] λ = stress/strain, where λ is the elastic modulus. The bulk modulus (B) describes volumetric elasticity. The shear modulus (G) describes a material's tendency to shear when acted upon by opposing forces, and Young's modulus (E) describes tensile elasticity. It is a measure of the stiffness of an elastic isotropic material and is a quantity used to characterize materials. Bulk modulus B and shear modulus G are calculated by the Voigt–Reuss–Hill approximation.[37–39] The Voigt and Reuss approximation of monoclinic symmetry is calculated using the following equations:[34]

$$B_V = \frac{1}{9}[C_{11} + C_{22} + C_{33} + 2(C_{12} + C_{13} + C_{23})], \quad (9)$$

$$B_R = \Omega(a + b + c + d + e + f)^{-1}, \quad (10)$$

$$a = (C_{33}C_{55} - C_{35}^2)(C_{11} + C_{22} - 2C_{12}), \quad (11)$$

$$b = (C_{23}C_{55} - C_{25}C_{35})(2C_{12} - 2C_{11} - C_{23}), \quad (12)$$

$$c = (C_{13}C_{35} - C_{15}C_{33})(C_{15} - 2C_{25}), \quad (13)$$

$$d = (C_{13}C_{55} - C_{15}C_{35})(2C_{12} + 2C_{23} - C_{13} - 2C_{22}), \quad (14)$$

$$e = 2(C_{13}C_{25} - C_{15}C_{23})(C_{25} - C_{15}), \quad (15)$$

$$f = C_{11}(C_{22}C_{55} - C_{25}^2) - C_{12}(C_{12}C_{55} - C_{15}C_{25}) + C_{15}(C_{12}C_{25} - C_{15}C_{22}) + C_{25}(C_{23}C_{35} - C_{25}C_{33}), \quad (16)$$

$$G_V = \frac{1}{15}[C_{11} + C_{22} + C_{33} + 3(C_{44} + C_{55} + C_{66}) - (C_{12} + C_{13} + C_{23})], \quad (17)$$

$$G_R = 15\left\{\frac{4(f + h + i + j + k + l)}{\Omega} + 3\left[\frac{g}{\Omega} + \frac{(C_{44} + C_{66})}{(C_{44}C_{66} - C_{46}^2)}\right]\right\}^{-1}, \quad (18)$$

$$h = (C_{33}C_{55} - C_{35}^2)(C_{11} + C_{22} + C_{12}), \quad (19)$$

$$i = (C_{23}C_{55} - C_{25}C_{35})(C_{11} - C_{12} - C_{23}), \quad (20)$$

$$j = (C_{13}C_{35} - C_{15}C_{33})(C_{15} + C_{25}), \quad (21)$$

$$k = (C_{13}C_{55} - C_{15}C_{35})(C_{22} - C_{23} - C_{12} - C_{13}), \quad (22)$$

$$l = (C_{13}C_{25} - C_{15}C_{23})(C_{15} - C_{25}), \quad (23)$$

The calculated elastic moduli of *Cm*-32 silicon and $P2_1/m$ silicon are listed in Table 3. The bulk moduli B of *Cm*-32 silicon and $P2_1/m$ silicon are both 79 GPa, which is slightly smaller than that of $Fd\bar{3}m$ silicon (88 GPa), and some new phases of our previous forecast of silicon, $C2/m$-16 silicon (82 GPa), $C2/m$-20 silicon (83 GPa), $I\bar{4}$ silicon (80 GPa)[6] and $P222_1$ silicon (83 GPa),[7] while slightly larger than *Amm*2 silicon (78 GPa)[6] and $P4_2/mnm$ silicon (74 GPa,[40] 75 GPa[41]). The shear modulus G of *Cm*-32 silicon is the smallest among the new silicon phases and our previous forecast of silicon ($C2/m$-16 silicon: 51 GPa; $C2/m$-20 silicon: 55 GPa; $I\bar{4}$ silicon: 48 GPa; *Amm*2 silicon: 51 GPa; $P222_1$ silicon: 54 GPa; $P4_2/mnm$ silicon: 48 GPa), while $P2_1/m$ silicon is only slightly smaller than $C2/m$-20 silicon. The bulk modulus B and shear modulus G of *Cm*-32 silicon and $P2_1/m$ silicon are both smaller than that of $Fd\bar{3}m$ silicon. Young's modulus E and Poisson's ratio ν can be expressed by the following equations: $E = 9BG/(3B + G)$, and $\nu = (3B - 2G)/(6B + 2G)$. The Young's modulus E of *Cm*-32 silicon is 118 GPa, and that of $P2_1/m$ silicon is 132 GPa, these values are both slightly smaller than that of $Fd\bar{3}m$ silicon, while the Poisson's ratios ν of *Cm*-32 silicon and $P2_1/m$ silicon are slightly larger than that of $Fd\bar{3}m$ silicon. In addition, the new allotropes in the silicon system are brittle with their values of B/G and ν smaller than 1.75 and 0.26 (a larger B/G value (more than 1.75) for a

Table 3 The calculated elastic modulus (GPa), hardness (GPa) and band gap (eV) of *Cm*-32 silicon, $P2_1/m$ silicon and $Fd\bar{3}m$ silicon

Space group	B	G	B/G	E	ν	H_v	E_g (HSE06)	E_g (PBE)
Cm-32	79	47	1.70	118	0.25	7.00	1.85	1.19
$P2_1/m$	79	54	1.48	132	0.22	12.45	0.83	0.26
$Fd\bar{3}m$	88	64	1.38	155	0.21	13.90	1.28	0.72
	98[a]					8[b], 9[c], 12.4[d], 2–16[e]	1.28[f]	

[a] Ref. 60. [b] Ref. 63. [c] Ref. 64. [d] Ref. 65. [e] Ref. 66. [f] Supplementary material of ref. 51 – HSE03.

solid represents ductility while a smaller B/G value (less than 1.75)[42] usually means that it is brittle. Like B/G value, Poisson's ratio v is consistent with B/G, but refers to ductile compounds, usually with a large v (more than 0.26)[43]). Meanwhile, $Fd\bar{3}m$ silicon is the most brittle, Cm-32 silicon is the least brittle.

Interest in the calculation of the Debye temperature Θ_D has been increasing in both semiempirical and theoretical phase diagram calculation areas since the Debye model offers a simple but high efficiency method to describe the phonon contribution to the Gibbs energy of crystalline phases. Debye temperature Θ_D is used to distinguish between high and low temperature regions for a solid. If $T > \Theta_D$, one expects all modes to have the energy of k_BT, but if $T < \Theta_D$, one expects the high-frequency modes to be frozen. The average sound velocity v_m and Debye temperature Θ_D can be approximately calculated using the following relations:[44,45]

$$\Theta_D = \frac{\hbar}{k_B}\left[\frac{3n}{4\pi}\left(\frac{N_A\rho}{M}\right)\right]^{\frac{1}{3}} v_m, \quad (24)$$

$$v_m = \frac{1}{3}\sum_{i=1}^{3}\int \frac{1}{v_i^3(\theta,\phi)}\frac{d\Omega}{4\pi} = \left[\frac{1}{3}\left(\frac{2}{v_l^3}+\frac{1}{v_t^3}\right)\right]^{-\frac{1}{3}}, \quad (25)$$

where $\hbar$ is Planck's constant, k_B is Boltzmann's constant, N_A is Avogadro's number, n is the number of atoms in the molecule, M is molecular weight, and ρ is the density, (θ, φ) are angular coordinates and $d\Omega = \sin\theta d\theta d\varphi$. If the elastic constants of the crystal are known, $v_i(\theta, \varphi)$ can be obtained by solving a secular equation, and v_m and Θ_D can then be calculated by numerical integration over θ and φ.[46,47] v_l and v_t are the longitudinal and transverse sound velocities, respectively, which can be obtained from Navier's equation:[48]

$$v_l = \sqrt{\left(B+\frac{4}{3}G\right)\frac{1}{\rho}}, \quad \text{and} \quad v_t = \sqrt{\frac{G}{\rho}}, \quad (26)$$

where B and G are bulk modulus and shear modulus, respectively. The calculated sound velocities and Debye temperatures of Cm-32 silicon, $P2_1/m$ silicon and $Fd\bar{3}m$ silicon are listed in Table 4. The longitudinal and transverse sound velocities of Cm-32 silicon and $P2_1/m$ silicon are smaller than those of $Fd\bar{3}m$ silicon, because Cm-32 silicon and $P2_1/m$ silicon have the smaller elastic moduli. The Debye temperature of Cm-32 silicon is 555 K and $P2_1/m$ silicon is 590 K at ambient pressure, and it is also smaller than that of $Fd\bar{3}m$ silicon (Θ_D = 639 K). For materials, usually, if its Debye temperature is higher than other materials, its hardness will be greater than other materials. So we calculated the hardness of Cm-32 silicon and $P2_1/m$ silicon using the Lyakhov and Oganov's model.[49] The calculated results are listed in Table 3. Consistent with previous predictions, the calculated hardness of Cm-32 silicon is 7.00 GPa, which is almost half that of $Fd\bar{3}m$ silicon (13.90 GPa). The calculated hardness of $P2_1/m$ silicon is 12.45 GPa, it is 43.78% greater than that of Cm-32 silicon, and 10.43% smaller than that of $Fd\bar{3}m$ silicon.

Table 4 The calculated density (ρ in g cm^{-3}), the longitudinal, transverse and mean elastic wave velocity (v_s, v_p, v_m in m s^{-1}), and the Debye temperature (Θ_D in K) for Cm-32 silicon, $P2_1/m$ silicon and $Fd\bar{3}m$ silicon

Space group	ρ	v_p	v_s	v_m	Θ_D
Cm-32	2.155	8108	4670	5186	555
$P2_1/m$	2.223	8241	4928	5454	590
$Fd\bar{3}m$	2.267, 2.329[a]	8744	5313	5870	639, 652[b], 636[c]

[a] Ref. 60 at 300 K. [b] Ref. 67. [c] Ref. 68.

Electronic structures

The band structures of Cm-32 silicon, $P2_1/m$ silicon and $Fd\bar{3}m$ silicon are calculated by GGA-PBE. It is known that the calculated band gap with DFT is usually underestimated by 30–50%, the true band gap must be larger than the calculated results. In consideration of this problem, Heyd *et al.* proposed a more tractable hybrid functional method, giving rise to the Heyd–Scuseria–Ernzerhof (HSE06) functional. The hybrid functional HSE06 is used in the form:[50,51]

$$E_{xc}^{HSE} = \mu E_x^{HF,SR}(\omega) + (1-\mu)E_x^{PW91,SR}(\omega) + E_x^{PW91,LR}(\omega) + E_c^{PW91}, \quad (27)$$

where the HF mixing parameter μ is 0.25 and the screening parameter providing good accuracy for the band gaps is ω = 0.207 Å^{-1}.[33,51] The calculated results of Cm-32 silicon, $P2_1/m$ silicon and $Fd\bar{3}m$ silicon are listed in Table 3. The results of HSE06 are much larger than that of PBE. The band gap of $Fd\bar{3}m$ silicon using the HSE06 is 1.28 eV in this work and ref. 52 with HSE03, which is very close to the experimental value (1.12 eV).[53] The band structures of Cm-32 silicon and $P2_1/m$ silicon are shown in Fig. 4. Cm-32 silicon and $P2_1/m$ silicon are both direct semiconductors with band gaps of 1.85 and 0.83 eV, respectively. At the GGA-PBE level of density functional theory, the $P2_1/m$ silicon is predicted to be a direct band gap semiconductor with a small band gap of 0.26 eV, as both the valence band maximum (VBM) and conduction band minimum (CBM) are located at the Γ point. This value of 0.26 eV is less than one third of the band gap (0.83 eV) of the HSE06 hybrid functional for $P2_1/m$ silicon. For Cm-32 silicon, the value of 1.19 eV is almost close to half of the band gap (1.85 eV) of the HSE06 hybrid functional. In addition, for $P2_1/m$ silicon, the energy at the B point is −0.33 eV and 1.02 eV near the Fermi level, so the direct band gap at the B point is 1.35 eV. Emphasis has obviously been given to direct band-gap materials, with gaps between 1.0 and 1.5 eV and with absorption spectra that strongly overlap with the solar spectrum.[54–56] These Si structures with different band gaps could be applied in single p–n junction thin-film solar cells or tandem photovoltaic devices.

Elastic anisotropy

The anisotropy of the crystal lattice along different directions, the atomic arrangement of the periodicity and the degree of density are not the same. This leads to the different physical and chemical properties of crystals in different directions, which are represented as the crystal anisotropy. The dependence of Young's modulus on the direction of load can be used as an example. Most materials exhibit anisotropic behavior. It is well known that the anisotropy of elasticity is an important implication

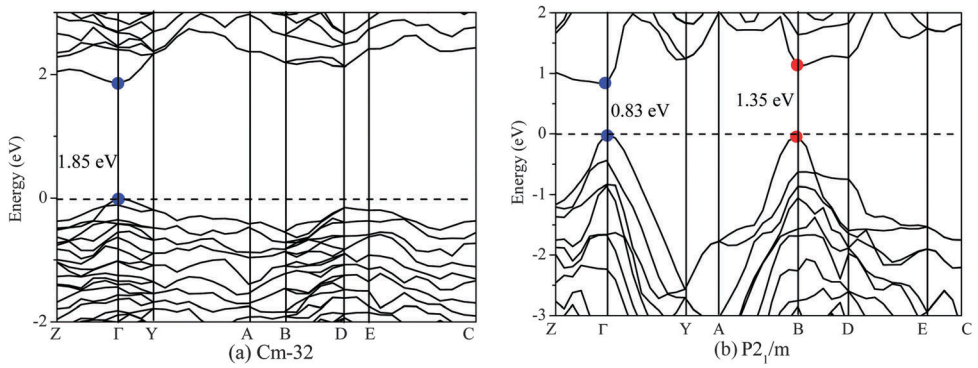

Fig. 4 Electronic band structure for the *Cm*-32 silicon (a) and $P2_1/m$ silicon (b) with HSE06.

in engineering science and crystal physics. In this paper, we mainly discuss the anisotropy of elastic modulus of materials. The directional dependence of the anisotropy is calculated by the Elastic Anisotropy Measures (ELAM)[57,58] code. The 3D figures of the Young's modulus for *Cm*-32 silicon and $P2_1/m$ silicon are shown in Fig. 5(a) and (b), and the 2D representation of the Young's modulus for *Cm*-32 silicon and $P2_1/m$ silicon are shown in Fig. 5(c) and (d). From the 3D figures of the Young's modulus for *Cm*-32 silicon and $P2_1/m$ silicon, all of them show different degrees of anisotropy. From Fig. 5(a) and (c), the maximum values and the minimum values of *Cm*-32 silicon and $P2_1/m$ silicon are 141 GPa, 101 GPa and 161 GPa, 100 GPa, respectively. The ratio E_{max}/E_{min} (*Cm*-32 silicon) = 1.40, and the ratio E_{max}/E_{min} ($P2_1/m$ silicon) = 1.61, in contrast, the ratio E_{max}/E_{min} ($Fd\bar{3}m$ silicon) = 183/124 = 1.48. The elastic anisotropy of $Fd\bar{3}m$ silicon is larger than that of *Cm*-32 silicon, while smaller than that of $P2_1/m$ silicon. More details of the anisotropy for Young's modulus are shown in two-dimensional figures (Fig. 5(c) and (d)).

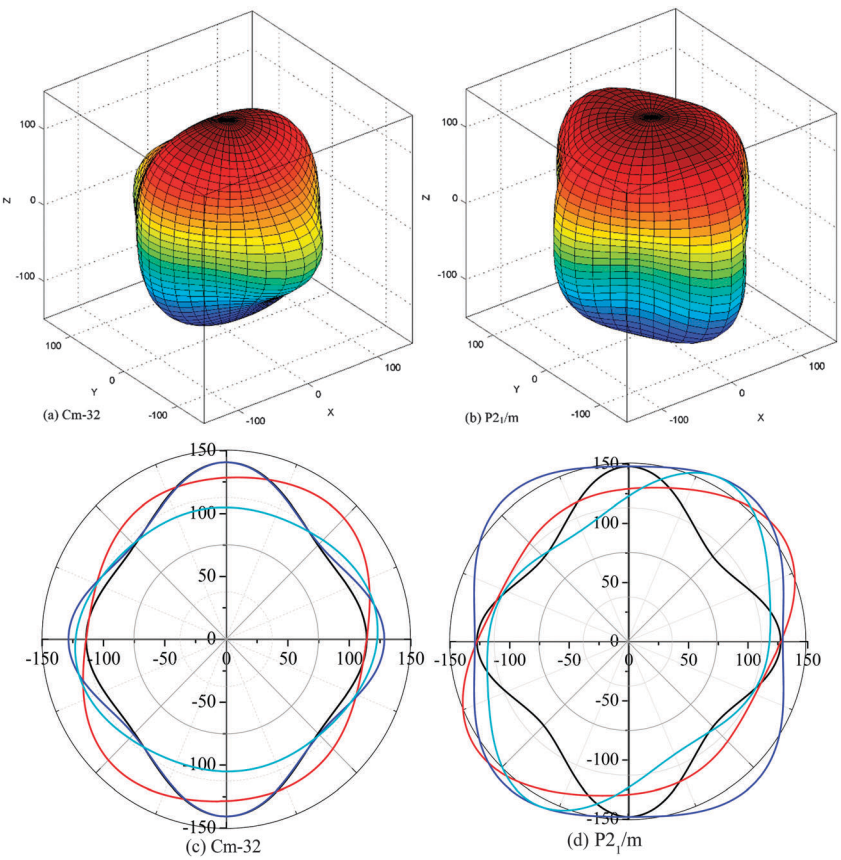

Fig. 5 The directional dependence of the Young's modulus for *Cm*-32 silicon (a) and $P2_1/m$ silicon (b), and 2D representation of Young's modulus in the (001), (010), (100) and (111) planes, for *Cm*-32 silicon (c) and $P2_1/m$ silicon (d). The black, red, blue and cyan solid lines represent the maximum and the dashed lines represent the (001), (010), (100) and (111) planes.

For *Cm*-32 silicon, the minimum values and the maximum values of the (001) plane, the (010) plane, the (100) plane and the (111) plane are 104 GPa, 141 GPa; 113 GPa, 136 GPa; 107 GPa, 141 GPa and 105 GPa, 123 GPa, respectively. It is obvious that the (100) plane has the most anisotropy, and the (111) plane has the least anisotropy. While for $P2_1/m$ silicon, the minimum values and the maximum values of the (001) plane, the (010) plane, the (100) plane and the (111) plane are 100 GPa, 148 GPa; 115 GPa, 157 GPa; 129 GPa, 160 GPa and 101 GPa, 158 GPa, respectively. It is obviously that for $P2_1/m$ silicon, the (111) plane has the most anisotropy, and the (100) plane has the least anisotropy. For $Fd\bar{3}m$ silicon, the E_{max}/E_{min} = 162/124 = 1.31 in the (001), (010) and (100) planes, while the E_{max}/E_{min} = 162/162 = 1.0 for the (111) plane, which shows that $Fd\bar{3}m$ silicon is isotropic in the (111) plane. From the above discussion, we note that the anisotropy of all the special planes for *Cm*-32 silicon and $P2_1/m$ silicon is smaller than that of the material itself. The anisotropy in Young's modulus of *Cm*-32 silicon for the (001) and (100) planes and $P2_1/m$ silicon for the (001) and (010) planes is slightly larger than that of $Fd\bar{3}m$ silicon, and the anisotropy in Young's modulus of *Cm*-32 silicon for the (010) plane and $P2_1/m$ silicon for the (100) plane is slightly smaller than that of $Fd\bar{3}m$ silicon. But the anisotropy of the (111) special plane for $Fd\bar{3}m$ silicon is smaller than that of the same plane for *Cm*-32 silicon and $P2_1/m$ silicon.

Optical properties

We then turn our interest on the absorption abilities of these two novel silicon allotropes. Absorption spectra of these allotropes are also calculated based on the HSE06 hybrid functional. The results are shown in Fig. 6 in comparison with that of the $Fd\bar{3}m$ silicon. According to the spectra range, we divided the spectrum into three parts, namely the infrared, visible and ultraviolet regions. We can see that both *Cm*-32 silicon and $P2_1/m$ silicon possess stronger absorption coefficients than $Fd\bar{3}m$ silicon in the photon energy range between 1.5 to 3.2 eV. For *Cm*-32 silicon and $P2_1/m$ silicon, the absorption of low-energy photons starts from about 1.2 eV and 0.6 eV, which is close to its direct band gap at the Γ point for $P2_1/m$ silicon. Moreover, *Cm*-32 silicon and $P2_1/m$ silicon exhibit higher optical absorption coefficients than $Fd\bar{3}m$ silicon when the photon energy is below 3.2 eV. This implies that *Cm*-32 silicon and $P2_1/m$ silicon can be the ideal candidates for photovoltaic materials. Our results suggest that *Cm*-32 silicon and $P2_1/m$ silicon are suitable for thin-film solar cell applications in view of their direct band gap characteristics and strong absorption abilities, if they can be synthesized in future experiments successfully.

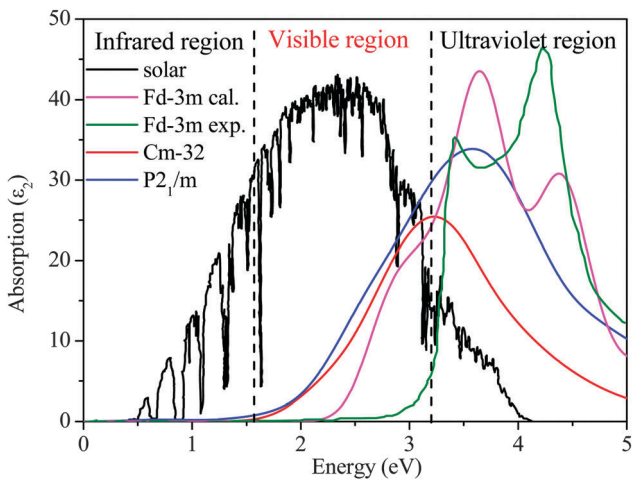

Fig. 6 Absorption spectra of *Cm*-32 silicon and $P2_1/m$ silicon compared to that of $Fd\bar{3}m$ silicon.

Minimum thermal conductivity

The conduction of heat in semiconductors has been the subject of intensive study during the past 60 years. From the practical point of view, thermal conductivity is an important parameter in determining the maximum power under which a semiconductor device may be operated. Moreover, thermal conductivity is one of the most important parameters determining the efficiency of those semiconductors used in thermoelectric energy conversion. The minimum thermal conductivity κ_{min} can be calculated using theoretical methods, namely, Cahill's model,[59] expressed as follows:

$$\kappa_{min} = \frac{k_B}{2.48} N^{2/3}(v_l + 2v_t) \quad (28)$$

In Cahill's model, N represents the number of atoms in a conventional volume and v_l and v_t represent the longitudinal and transverse sound velocities, respectively. Cahill *et al.* deduced the κ_{min} as a function of temperature, which can be expressed by the following form:

$$\kappa_{min} = \left(\frac{\pi}{6}\right)^{1/3} k_B n^{2/3} \sum_i v_i \left(\frac{T}{\Theta_i}\right)^2 \int_0^{\Theta_i/T} \frac{x^3 e^x}{(e^x - 1)^2} dx \quad (29)$$

The sum is obtained from the three acoustic mode (two transverse and one longitudinal) speeds of v_i. Θ_i is the cutoff frequency for each polarization expressed in K, $\Theta_i = v_i[h/(2\pi k_B)](6\pi^2 n)^{1/3}$, and n is the number density of atoms. Utilizing eqn (28) and (29), the κ_{min} *versus* temperature for *Cm*-32 silicon and $P2_1/m$ silicon is plotted in Fig. 7. The thermal conductivities increase with temperature and eventually reach corresponding stable values. At low temperature (about 0–200 K), their κ_{min} are similar to each other. At high temperature (T > 1200 K), minimum thermal conductivity is almost constant, it increases linearly with temperature at high temperatures. Among two novel silicon allotropes and $Fd\bar{3}m$ silicon, $Fd\bar{3}m$ silicon owns the highest value and is slightly higher than that of *Cm*-32 silicon and $P2_1/m$ silicon, while *Cm*-32 silicon owns the lowest value. At T = 300 K, the minimum thermal conductivity κ_{min} of $Fd\bar{3}m$ silicon is 1.13 W cm^{-1} K^{-1}, the value is slightly smaller than the available theoretical value (1.56 W cm^{-1} K^{-1}).[60] In addition, the minimum thermal conductivity κ_{min} of *Cm*-32 silicon and $P2_1/m$ silicon are very close to the minimum thermal conductivity of $Fd\bar{3}m$ silicon, these two novel silicon allotropes also have good thermal conductivity.

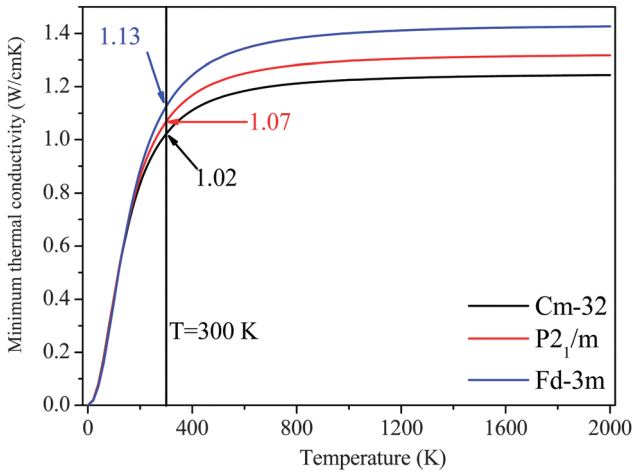

Fig. 7 κ_{min} of *Cm*-32 silicon and $P2_1/m$ silicon as a function of temperature.

IV. Summary

The stability, structural, elastic, elastic anisotropic, optical and electronic properties and minimum thermal conductivity of *Cm*-32 silicon and $P2_1/m$ silicon are systematically investigated in this paper. *Cm*-32 silicon and $P2_1/m$ silicon are thermodynamically, mechanicallly and dynamically stable. The most striking feature of *Cm*-32 silicon and $P2_1/m$ silicon is their direct band gaps, with values of 1.85 and 0.83 eV, respectively. Both the VBM and CBM of *Cm*-32 silicon and $P2_1/m$ silicon are located at the Γ point, while for $P2_1/m$ silicon, there is another direct band gap with a value of 1.35 eV at the *B* point. The elastic anisotropy calculations of *Cm*-32 silicon and $P2_1/m$ silicon shows that $P2_1/m$ silicon exhibits larger anisotropy than $Fd\bar{3}m$ silicon, while *Cm*-32 silicon exhibits smaller anisotropy than $Fd\bar{3}m$ silicon. For the absorption abilities of these two novel silicon allotropes, they both possess stronger absorption coefficients than $Fd\bar{3}m$ silicon in the visible region. Our results suggest that *Cm*-32 silicon and $P2_1/m$ silicon are suitable for thin-film solar cell applications in view of their direct band gap characteristics and strong absorption abilities. At $T = 300$ K, the minimum thermal conductivity κ_{min} of *Cm*-32 silicon and $P2_1/m$ silicon is as good as that of $Fd\bar{3}m$ silicon. *Cm*-32 silicon and $P2_1/m$ silicon can be expected to be multifunctional materials with direct band gaps and good hydrogen storage abilities.

Acknowledgements

This work was supported by the Natural Science Foundation of China (No. 61474089), Open fund of key laboratory of complex electromagnetic environment science and technology, China Academy of Engineering Physics (No. 2015-0214. XY.K).

References

1 B. Petter Jelle, C. Breivik and H. Drolsum Røkenes, *Sol. Energy Mater. Sol. Cells*, 2012, **100**, 69–96.
2 M. S. Hybertsen and S. G. Louie, *Phys. Rev. Lett.*, 1985, **55**, 1418.
3 J. Besson, E. Mokhtari, J. Gonzalez and G. Weill, *Phys. Rev. Lett.*, 1987, **59**, 473.
4 B. D. Malone, J. D. Sau and M. L. Cohen, *Phys. Rev. B: Condens. Matter Mater. Phys.*, 2008, **78**, 035210.
5 Z. Zhao, F. Tian, X. Dong, Q. Li, Q. Q. Wang, H. Wang, X. Zhong, B. Xu, D. L. Yu, J. L. He, H. T. Wang, Y. M. Ma and Y. J. Tian, *J. Am. Chem. Soc.*, 2012, **134**, 12362.
6 Q. Y. Fan, C. C. Chai, Q. Wei, H. Y. Yan, Y. B. Zhao, Y. T. Yang, X. H. Yu, Y. Liu, M. J. Xing, J. Q. Zhang and R. H. Yao, *J. Appl. Phys.*, 2015, **118**, 185704.
7 Q. Y. Fan, C. C. Chai, Q. Wei, Y. T. Yang, Q. Yang, P. Y. Chen, M. H. Xing, J. Q. Zhang and R. H. Yao, *J. Solid State Chem.*, 2016, **233**, 471–483.
8 A. De and C. E. Pryor, *J. Phys.: Condens. Matter*, 2014, **26**, 045801.
9 S. Cahangirov, M. Topsakal, E. Aktürk, H. Şahin and S. Ciraci, *Phys. Rev. Lett.*, 2009, **102**, 236804.
10 S. Botti, J. A. Flores-Livas, M. Amsler, S. Goedecker and M. A. L. Marques, *Phys. Rev. B: Condens. Matter Mater. Phys.*, 2012, **86**, 121204.
11 H. J. Xiang, B. Huang, E. J. Kan, S. H. Wei and X. G. Gong, *Phys. Rev. Lett.*, 2013, **110**, 118702.
12 J. Lee, H. A. Scheraga and S. Rackovsky, *J. Comput. Chem.*, 1997, **18**, 1222–1232.
13 J. Lee, I. H. Lee and J. Lee, *Phys. Rev. Lett.*, 2003, **91**, 080201.
14 I.-H. Lee, J. Lee, Y. J. Oh, S. Kim and K. J. Chang, *Phys. Rev. B: Condens. Matter Mater. Phys.*, 2014, **90**, 115209.
15 M. S. Hybertsen and S. G. Louie, *Phys. Rev. B: Condens. Matter Mater. Phys.*, 1986, **34**, 5390.
16 L. Hedin, *J. Phys.: Condens. Matter*, 1999, **11**, R489–R528.
17 Q. Q. Wang, B. Xu, J. Sun, H. Y. Liu, Z. S. Zhao, D. L. Yu, C. Z. Fan and J. L. He, *J. Am. Chem. Soc.*, 2014, **136**, 9826.
18 A. Mujica, C. J. Pickard and R. J. Needs, *Phys. Rev. B: Condens. Matter Mater. Phys.*, 2015, **91**, 214104.
19 M. Amsler, S. Botti, M. A. L. Marques, T. J. Lenosky and S. Goedecker, *Phys. Rev. B: Condens. Matter Mater. Phys.*, 2015, **92**, 014101.
20 Y. G. Guo, Q. Wang, Y. Kawazoe and P. Jena, *Sci. Rep.*, 2015, **5**, 14342.
21 Y. J. Oh, I. H. Lee, S. Kim, J. Lee and K. J. Chang, *Sci. Rep.*, 2015, **5**, 18086.
22 X. X. Zhang, Y. C. Wang, J. Lv, C. Y. Zhu, Q. Li, M. Zhang, Q. Li and Y. M. Ma, *J. Chem. Phys.*, 2013, **138**, 114101.
23 I. H. Lee, Y. J. Oh, S. Kim, J. Lee and K. J. Chang, *Comput. Phys. Commun.*, DOI: 10.1016/j.cpc.2016.02.011.
24 P. Hohenberg and W. Kohn, *Phys. Rev.*, 1964, **136**, B864.
25 W. Kohn and L. J. Sham, *Phys. Rev.*, 1965, **140**, A1133.
26 D. Vanderbilt, *Phys. Rev. B: Condens. Matter Mater. Phys.*, 1990, **41**, 7892.
27 S. J. Clark, M. D. Segall, C. J. Pickard, P. J. Hasnip, M. I. J. Probert, K. Refson and M. C. Payne, *Z. Kristallogr.*, 2005, **220**, 567.
28 J. P. Perdew, K. Burke and M. Ernzerhof, *Phys. Rev. Lett.*, 1996, **77**, 3865.
29 D. M. Ceperley and B. J. Alder, *Phys. Rev. Lett.*, 1980, **45**, 566.
30 J. P. Perdew and A. Zunger, *Phys. Rev. B: Condens. Matter Mater. Phys.*, 1981, **23**, 5048.

31 B. G. Pfrommer, M. Côté, S. G. Louie and M. L. Cohen, *J. Comput. Phys.*, 1997, **131**, 233–240.
32 H. J. Monkhorst and J. D. Pack, *Phys. Rev. B: Solid State*, 1976, **13**, 5188.
33 A. V. Krukau, O. A. Vydrov, A. F. Izmaylov and G. E. Scuseria, *J. Chem. Phys.*, 2006, **125**, 224106.
34 Z. J. Wu, E. J. Zhao, H. P. Xiang, X. F. Hao, X. J. Liu and J. Meng, *Phys. Rev. B: Condens. Matter Mater. Phys.*, 2007, **76**, 054115.
35 Q. Y. Fan, Q. Wei, H. Y. Yan, M. G. Zhang, D. Y. Zhang and J. Q. Zhang, *Acta Phys. Pol., A*, 2014, **126**, 740–746.
36 D. R. Askeland and P. P. Phulé, *The Science and Engineering of Materials*, 5th edn, 2006, p. 198.
37 W. Voigt, *Lehrburch der Kristallphysik*, Teubner, Leipzig, 1928.
38 A. Reuss, *Z. Angew. Math. Mech.*, 1929, **9**, 49.
39 R. Hill, *Proc. Phys. Soc., London*, 1952, **65**, 349.
40 M. C. Nguyen, X. Zhao, C. Z. Wang and K. M. Ho, *Phys. Rev. B: Condens. Matter Mater. Phys.*, 2014, **89**, 184112.
41 Q. Y. Fan, C. C. Chai, Q. Wei, Q. Yang, P. K. Zhou, M. J. Xing and Y. T. Yang, *Mater. Sci. Semicond. Process*, 2016, **43**, 187–195.
42 S. F. Pugh, *Philos. Mag.*, 1954, **45**, 823.
43 J. J. Lewandowski, W. H. Wang and A. L. Greer, *Philos. Mag. Lett.*, 2005, **85**, 77.
44 O. L. Anderson, *J. Phys. Chem. Solids*, 1963, **24**, 909–917.
45 Q. Y. Fan, Q. Wei, H. Y. Yan, M. G. Zhang, Z. X. Zhang, J. Q. Zhang and D. Y. Zhang, *Comput. Mater. Sci.*, 2014, **85**, 80–87.
46 O. L. Anderson, *Physical Acoustics*, Academic Press, New York, vol. III(part B), 1965.
47 G. Grimvall, *Thermophysical Properties of Materials*, North-Holland, Amsterdam, 1986.
48 K. B. Panda and K. S. Ravi, *Comput. Mater. Sci.*, 2006, **35**, 134–150.
49 A. O. Lyakhov and A. R. Oganov, *Phys. Rev. B: Condens. Matter Mater. Phys.*, 2011, **84**, 092103.
50 J. Heyd, G. E. Scuseria and M. Ernzerhof, *J. Chem. Phys.*, 2003, **118**, 8207–8215.
51 J. Heyd, G. E. Scuseria and M. Ernzerhof, *J. Chem. Phys.*, 2006, **124**, 219906.
52 J. Heyd, J. E. Peralta, G. E. Scuseria and R. L. Martin, *J. Chem. Phys.*, 2005, **123**, 174101.
53 M. Shishkin and G. Kresse, *Phys. Rev. B: Condens. Matter Mater. Phys.*, 2007, **75**, 235102.
54 J. Vidal, S. Botti, P. Olsson, J. F. Guillemoles and L. Reining, *Phys. Rev. Lett.*, 2010, **104**, 056401.
55 S. Botti, D. Kammerlander and M. A. L. Marques, *Appl. Phys. Lett.*, 2011, **98**, 241915.
56 I. Aguilera, J. Vidal, P. Wahnón, L. Reining and S. Botti, *Phys. Rev. B: Condens. Matter Mater. Phys.*, 2011, **84**, 085145.
57 A. Marmier, Z. A. D. Lethbridge, R. I. Walton, C. W. Smith, S. C. Parker and K. E. Evans, *Comput. Phys. Commun.*, 2010, **181**, 2102–2115.
58 Q. Y. Fan, Q. Wei, C. C. Chai, H. Y. Yan, M. G. Zhang, Z. Z. Lin, Z. X. Zhang, J. Q. Zhang and D. Y. Zhang, *J. Phys. Chem. Solids*, 2015, **79**, 89–96.
59 D. G. Cahill, S. K. Watson and R. O. Pohl, *Phys. Rev. B: Condens. Matter Mater. Phys.*, 1992, **46**, 6131.
60 S. Adachi, *Handbook on physical properties of semiconductors*, Springer, 2004, vol. 1.
61 E. R. Cohen and B. N. Taylor, *Rev. Mod. Phys.*, 1987, **59**, 1121.
62 H. J. McSkimin and P. Andreatch, Jr., *J. Appl. Phys.*, 1964, **35**, 2161.
63 J. J. Gilman, *J. Appl. Phys.*, 1975, **46**, 5110.
64 B. R. Lawn, A. G. Evans and D. B. Marshall, *J. Am. Ceram. Soc.*, 1980, **63**, 574.
65 S. Danyluk, D. S. Lim and J. Kalejs, *J. Mater. Sci. Lett.*, 1985, **4**, 1135.
66 P. Feltham and R. Banerjee, *J. Mater. Sci.*, 1992, **27**, 1626.
67 H. Siethoff and K. Ahlborn, *Phys. Status Solidi B*, 1995, **190**, 179.
68 O. Madelung, *Semiconductors: Data Handbook*, Springer, 3rd edn, 2004.